Biopolymer blends from hardwood lignin and bio-polyamides: Compatibility and miscibility

R.Muthuraj, M. Hajee, A.R Horrocks and B.K Kandola*

Institute for Materials Research and Innovation
University of Bolton, Deane Road, Bolton, BL3 5AB, UK

**Corresponding author. Tel: +44 1204 903517; E-mail address:* B.Kandola@bolton.ac.uk

Abstract

The compatability of hardwood lignin (TcA)/bio-polyamide (PA) blends, prepared by melt compounding TcA with three different biobased polyamides, PA 1012, PA 1010 and PA 11 in a twin screw extruder have been studied. FTIR studies indicated the existence of physicochemical interactions between the TcA and polyamide. The melting temperatures of the blends were significantly reduced compared to the respective neat polyamides, which was attributed to the enhanced compatibility between the two components. The compatibility was also attributed to the increased glass transition (T_g) of the polyamide. Thermogravimetric studies, while not indicating any interaction during the processing stage, suggested that there was some during the thermal degradation stage, which assisted formation of carbonaceous residue. The addition of each polyamide to TcA considerably reduced its viscosity and enhanced its processability even at high lignin contents. Morphological analysis showed that heterogeneity for all the blends was quite uniform, although TcA domain sizes were considerably smaller (~ 0.5 μm) in the PA11 matrix compared to those in PA1010 and PA1012, suggesting better compatibility in the TcA/PA11 blends. This observation was consistent with the thermodynamic Gibbs' free enery values of the respective blends. Overall, the order of blend compatibility was TcA/PA11 > TcA/PA1010 > TcA/PA1012.

Keywords: Lignin, bio-polyamides, compatibility

1. Introduction

Bio-polymers have created great interest both in industry and academia due to the desire to reduce carbon dioxide emissions from processing petrochemical feedstock and increasing interest in alternative, sustainable solutions in the production of polymeric and composite materials [1,2]. This is exemplified by the desire to exchange petrochemically-based precursors such as acrylic copolymers for production of carbon fibres by alternative bio-based, carbon-containing materials such as lignin [3,4]. However, production of bio-based polymers still proves to be expensive and often produces inferior properties compared to commodity/synthetic polymers derived from petrochemicals [2,5]. Lignin is an aromatic natural polymer which is the second most abundantly available natural polymer after cellulose [4]. It is produced in large quantities as an inexpensive by-product from the paper and cellulosic bioethanol industries [6]. Different types of extractions (e.g. Kraft, sulphite, organosolv, steam explosion) are used to extract the lignin from lignocellulosic materials [7] and these extraction methods determine the chemical structure and properties of the resulting lignin [4]. Lignin so far has not found any high value-added application [8] owing to its amorphous nature and brittleness. However, blending lignin with other bio-derived, thermoplastic polymers could find potential applications as engineering polymers.

Melt blending is physical blending or simple mixing of polymeric materials in the melt state with no chemical reactions taking place. If melt blending is to be used as a convenient route to create new materials, it is essential that maximising the blend homogeneity is a crucial element in determining optimal properties for each desired combination [9]. The aim of this work is to increase the compatibility and hence processability of the lignin/biopoly amide

blends with the ultimate objective of maximising their ease of melt processing into filaments having acceptable tensile properties.

The open literature describes the structure, interactions and properties of many such polymer/lignin blends [9–17]. Compatibility is of key importance in determining not only the ease of blend processing but also final blends properties. For example, polypropylene (PP)/lignin blends are reported to be incompatible, showing heterogeneous phase morphology with large lignin domains in the PP resulting matrix resulting in poor mechanical performance [18]. Unlike PP/lignin blends, blends of lignin with polymers composed of aromatic moieties (polystyrene (PS), polycarbonate (PC) and poly(ethylene-terephthalate) (PET)) show better compatibility and improved properties with smaller lignin domains in the polymer matrix [18]. These polymers are not hydrogen-bonding, and so the observed compatibility in these blends is due to the π-electron interactions between the two components. However, hydrogen bonding formation is observed in the blends of lignin and several biopolymers such as polyhydroxybutyrate (PHB) and poly(butylene adipate-co-terephthalate) (PBAT) and free phenolic –OH groups present in lignin which enable greater component miscibility. PHB has been claimed to form a miscible blend with up to 40 wt.% lignin content, but phase separation occurs with higher lignin concentrations [19,20]. The compatibility of PBAT with lignin is better because the two polymers also have additional π-π electron interactions [21]. Liu and Conxiu *et al.* [22,23] reported that poly(vinyl pyrrolidone) is miscible with lignin. A similar conclusion was drawn about lignin/polyaniline blends by Rodrigues et al. [24]. Another polymer found to be miscible with lignin is poly(ethylene oxide) (PEO). Based on FTIR spectra and the composition dependence of the glass transition temperature (T_g) of the blends, Kadla and Kubo [25–28] concluded that miscibility is the result of the formation of H-bonds between the ether groups of PEO and the hydroxyl and carboxyl groups of lignin. Lignin/polyamide compatible blends also have been recently reported, as would be expected, due to the hydrogen-

bonding nature of polyamides [29,30]. Furthermore, recent investigations suggest that polyamides can act as a char forming-agent [31]. Therefore, it can be hypothesized that producing precursor fibre from lignin/polyamide blends can enhance the yield of the resulting carbon fibre besides increasing melt processability of the lignin.

This work builds on this previous work and studies the compatibilities of blends of lignin with the different bio-based polyamides, PA 1012, PA 1010 and PA 11. TcA was blended with PA1012, PA1010 and PA11 to study their compatibility in terms of ease of processability, thermal stability and morphological properties.

2. Materials and Methods

2.1 Materials

Lignin: Unmodified organosolv hardwood lignin (TcA, sourced from Tecnaro, Ilsfeld, Germany) with weight average molecular weight (M_w) of 3952 g/mol, polydispersity index (PDI) of 4.69, a T_g of 100ºC and phenolic hydroxyl (OH_{ph}) group content of 2.4 mmol/g [4]. The detailed analysis of TcA is provided elsewhere [4].

Polyamides: PA1012 (Vestamid® Terra DD, Evonik Industries, Germany), PA1010 (Vestamid® Terra DS, Evonik Industries, Germany) and PA11 (BMNO, Rislan, Arkema, France).

2.2 Lignin/polyamide blend preparation

Prior to melt compounding, both lignin and polyamides were dried at 80ºC overnight in an oven. Melt blending at laboratory scale was performed in a twin-screw compounder (Prism Eurolab 16, Thermo Fisher Scientific). For all the blend preparations, the temperature profile varied between 140 and 190°C, with a screw speed of 100 rpm. The resulting extrudates

were pelletized after cooling in a water bath. To prepare blends with TcA concentrations >50 wt.% and principally 70 wt.%, the blends were compounded in two steps. In the first step, TcA/PA 50/50 wt.% blends were prepared and dried at 80ºC overnight. Subsequently, more TcA was added into 50/50 wt.% blend to increase the TcA concentration to a maximum 70 wt.% in the resulting blends (Table 1). All percentage concentrations are on a weight/weight basis.

Since the aim of this work was to produce the lignin/bio-polyamide blends with a maximum amount of lignin for carbon fiber production, the series of TcA/PA blends listed in Table 1 were produced. TcA/PA1012, TcA/PA101 and TcA/PA11 blends showed ease in the processability up to 70 wt.% lignin incorporation and their respective processabilities were similar. Based on these observations it could be assumed that TcA/PA11 (60/40) blend processability will be similar to TcA/PA1012 (60/40) and TcA/PA1010 (60/40). Therefore, this study ruled out the TcA/PA11 60/40 blends to simplify the matrix

Table 1. Compounding temperature and compounding steps of the produced TcA blends with different bio-polyamides

Samples	Composition (wt.%)		Compounding		
	TcA	Polyamide	Temperature profile (ºC)	One step/ two steps	Processability
TcA/PA1012					
TcA/PA1012 (30/70)	30	70	180;190;190;190;190;185	One step	✔
TcA/PA1012 (40/60)	40	60	180;190;190;190;190;185	One step	✔
TcA/PA1012 (50/50)	50	50	180;190;190;190;190;185	One step	✔
TcA/PA1012 (60/40)	60	40	180;190;190;190;190;185	Two steps	✔
TcA/PA1012 (70/30)	70	30	180;190;190;190;190;185	Two steps	✔
TcA/PA1010					
TcA/PA1010 (50/50)	50	50	180;190;190;190;190;185	One step	✔

TcA/PA1010 (60/40)	60	40	180;190;190;190;190;185	Two steps	✔
TcA/PA1010 (70/30)	70	30	180;190;190;190;190;185	Two steps	✔
TcA/PA11					
TcA/PA11 (50/50)	50	50	180;190;190;190;190;185	One step	✔
TcA/PA11 (70/30)	70	30	180;190;190;190;190;185	Two steps	✔

2.3 Characterisation

Infrared attenuated reflection spectroscopy (FTIR-ATR): FTIR spectra were acquired using an IR-ATR, Nicolet iS10 (Thermo Scientific) with a Smart iTR attachment used with single reflection diamond crystal. Dried TcA powder and thin slices of pellets of polyamides and melt compounded blends were used for the analysis. The spectra were recorded with 32 scans and 4 cm^{-1} resolution.

Thermal Analysis: The melting temperature (T_m), crystallization temperature (T_c), cold crystallization temperature (T_{cc}) and crystallinity percentage were determined via Differential Scanning Calorimetry, DSC, (TA Q2000, TA instruments, UK). The DSC analysis was performed under nitrogen on TcA powder and pellets of TcA/PAs blends with a sample size of around 5-7 mg. A heat-cool-heat run was performed with heating and cooling rates of 10°C/min under controlled nitrogen atmosphere (50 mL/min). The percentage of the crystallinity of the polyamide was calculated as follows:

$$\text{Crystallinity (\%)} = \frac{\Delta H_m}{\Delta H_m{}^o{}_{(1-W_f)}} \; x\; 100 \qquad \text{(Eqn. 1)}$$

where ΔH_m is melting enthalpy derived from the area under a given DSC melting endotherm and $\Delta H_m{}^o$ is the theoretical melting enthalpy of 100% crystalline polyamide (PA1012: 209.2

J/g; PA1010: 244 J/g and PA11: 226.4 J/g) [32,33]. W_f is the weight fraction of TcA in the blends.

The thermal stability in terms of onset of thermal degradation temperature taken as the temperature where 5% mass loss occurs and residual mass at different temperatures was determined via thermogravimetric analysis, TGA, (SDT-Q600, TA instruemnts, UK). The TGA analysis was performed (sample size 8-10 mg) in a nitrogen atmosphere (50 mL/min) with a heating rate of 20°C/minute.

Dynamic Mechanical Analysis (DMA): A DMA Q8000 (TA instruments, UK) instrument was used to analyse the thermal transitions of the lignin, polyamide and their blends in pellet form. Around 2 g pellets were sandwiched between rigid aluminium plates (thickness: 0.6 mm) and then a thin aluminium foil (thickness: 0.05mm) was used to wrap them to avoid sample loss during the experiment. The Tan δ peak was considered as the second order thermal transition (T_g) of each sample. The measurements were performed in a single cantilever mode from room temperature to 140ºC with a heating rate of 3 ºC/min, 1 Hz frequency and an oscillation amplitude of 15 µm.

Rheological analysis: A Discovery Hybrid Rheometer HR2 equipped with an environmental control chamber (TA instruments, UK) was used to observe the rheological properties of the lignin, polyamide and their blends. Prior to testing the samples, the samples were dried at 85ºC for a few hours to minimize the moisture content in the samples. The dried samples were placed between 25 mm diameter parallel-plate geometry with a gap of 1000 µm. Dynamic frequency sweep tests were performed at 200ºC for all the samples from higher (628 rad/s) to lower (0.1 rad/s) frequency with 2% constant strain.

Morphological Analysis: Extruded strands were brittle enough to be manually fractured for SEM analysis. The cross-sectional morphologies of the fractured strands were examined

using a Hitachi S-3400N scanning electron microscope with an accelerating voltage of 5 kV. In order to reduce the charging during imaging, the samples were gold coated prior to observing the morphology. The dispersed TcA domain sizes in each polyamide blend was measured using Image J software with 64-bit Java 1.8.0_112 using a pre-calibrated scale bar. The reported domain sizes were averages of at least 30-40 measurements.

2.4 Theoretical analysis of the miscibility and compatibility

The interaction between the blended polymers can be analysed in terms of Gibb's free energy [34]:

$$\Delta G_m = \Delta H_m - T\Delta S_m \qquad \text{(Eqn. 2)}$$

where ΔG_m is Gibbs free energy of mixing, ΔH_m is enthalpy of mixing, T is absolute temperature and ΔS is mixing entropy. A negative ΔG_m must be observed in the polymer blends when they have achieved miscibility or intimate mixing. Therefore, ΔG_m values of the polymer blends are largely dependent on ΔH_m while to a lesser extent on ΔS_m. ΔH_m and ΔS_m values of the polymer blends are influenced by specific interactions of the polymers, and respective molecular weights and solubility parameters. In polymer blends, phase separation is favoured when ΔS_m is small. However, there are many polymers which have been found to be miscible with a small ΔS_m value. Such a phenomenon has been attributed to the hydrogen bonding, π-π complex formation, charge transfer and ionic interactions between the blended polymers [35].

Molecular weight of the polymer also determines the magnitude of ΔS_m and due to the high randomness of the low molecular weight polymers, the resulting higher entropy in polymer blends leads to miscibility favouring a negative free energy ΔG formation by endothermic heat of mixing [35]. When high molecular weight polymers are mixed, it is very rare to get higher ΔS_m values because random mixing is nearly impossible Therefore, ΔS_m is negligible in such blend systems [35].

The solubility parameter (δ) is a measure of the cohesion of a material. The relationship between ΔH_m and δ can be expressed as [34]:

$$\Delta H_m = (\delta_1 - \delta_2)^2 \ \varphi_1 \varphi_2 \qquad \text{(Eqn. 3)}$$

where δ_1 and δ_2 are the solubility parameter values of two components while φ_1 and φ_2 are the volume fractions of the respective components. Equation 3 suggests that the two components can be miscible when solubility parameters of both components are perfectly matched. The solubility parameter (δ) of the components can be calculated as [34]:

$$\delta = (\rho \sum G_m)/M \qquad \text{(Eqn. 4)}$$

where M is the molecular weight of a repeat unit and ρ and G_m are density and group molar attraction constants of the polymer, respectively.

3. Results and Discussions

In order to identify and/or quantify any blend component physicochemical interactions occurring in each of the ten blends in Table 1, their existence has been identified in the first instance via FTIR, changes in individual component thermophysical characteristics via DSC, component interactions that may indicate the blend suitability as a carbon fibre precursor via TGA, blend melt viscosity versus processability characteristics via rheometry and blend morphology via SEM. Each of these issues are discussed below.

3.1 FTIR Spectroscopy

The full range FTIR spectrum of TcA shown in Figure 1(a) is similar to typical spectra of lignin as reported in the literature [36,37]. An extensive FTIR analysis of the TcA have been recently reported by Culebras *et al.* [4]. Briefly, the TcA higher energy spectral region shows

a broad distinctive band at 3390-3460 cm^{-1}, which is attributed to phenolic and aliphatic hydroxyl groups, methyl and methylene C-H stretching vibration peaks at 3000-2840 cm^{-1}, conjugated aldehydic and carboxylic acidic C=O stretching peaks observed over the range 1698 cm^{-1} [4]. The peaks at 1326 cm^{-1} and 1210 cm^{-1} are typical aromatic syringyl and aromatic guaiacyl ether linkages, respectively [4]. The full range FTIR spectra of neat PA1012, PA1010, PA11 and TcA/polyamide blends are also shown in Figures 1(a) and-(b). The polyamide (PA1012, PA1010 and PA11) and TcA/PA blend spectra each showed a broad peak at ~3300 cm^{-1}, which corresponds to the N-H stretching vibration as part of the concerted amide group frequency bands where broadening in TcA/PA blends is indicative of H-bonding [38,39]. For the polyamides, symmetric and asymmetric C-H stretching vibrations of methylene group peaks were observed at 2919 and 2851 cm^{-1}, respectively [40]. The peak at 1633-1640 cm^{-1} in the PA1012, PA1010 and PA11 spectra (Figures 1(c), (e) and (g)) was assigned to the so-called amide I (C=O mode) [38,39,41]. The band at 1535 cm^{-1} in the PA1010 (Figure 1(e)) is associated with the N-H (amide II) bending vibration [32,39]. This band appears at a slightly higher frequency (1540 cm^{-1}) in PA1012 and PA11 (Figures 1(c) and (g)). The peak at 1462 cm^{-1} in the PA1010, PA11 and PA1012 spectra (Figures 1(c), (e) and (g)) was attributed to the C-N stretching vibration of the amide groups [41]. The absorbance peak structure in the range of 1300-1200 cm^{-1} may be related to N-H and C-H twisting of PA1012 and PA11 (Figures 1(d) and (h)) [40,42].

Because interactions between the blended components in the blend can often be analysed by FTIR, the characteristic peaks of the TcA/biopolyamide blends were compared with those of TcA and respective neat biopolyamide spectra after normalization with respect to the maximum intensity peak of the reference TcA sample spectrum. Blend FTIR-IR spectra from the 1800-1450 cm^{-1} and 1400-1150cm^{-1} regions are shown in Figures 1 (c)-(h), which suggest that there are significant differences in the characteristic peaks of the pure TcA and

polyamide spectra. For example, the aldehyde and carboxylic acid group peaks of the TcA were shifted to higher wave numbers in the presence of PA1012, PA1010 and PA11 (see Table 2). Similarly, the TcA aromatic ether bond peak at 1210 cm^{-1} was also shifted to higher wave numbers (Table 2). Culebras *et al.* [4] reported that the ether bond of the TcA can shift to higher wave numbers because of crosslinking when exposed to 200ºC for about 1 hour. Such crosslinking may not be possible in our TcA/PA blends because the blends were prepared with short compounding cycle times (~2 min) at 200ºC. However, further evidence for onset of crosslinking of TcA is presented in the rheology section below. The characteristic peaks of polyamides (amide II (N-H) and amide I (C=O)) peaks absorbance maxima were shifted to higher wavenumbers by about 3-4 cm^{-1} after incorporation of TcA (Table 2). These observed characteristic peak shifts in the blend samples indicate a degree of interaction between each polyamide and TcA. If this resulted in formation of lignin-PA crosslinks, then the linear polyamide molecular chain sequences in the resulting blend would be reduced in length, leading to a reduction in the melting behaviour of the blends, which is corroborated by DSC analysis in the following section. Similar observations have already been reported in polyamide blend systems [29].

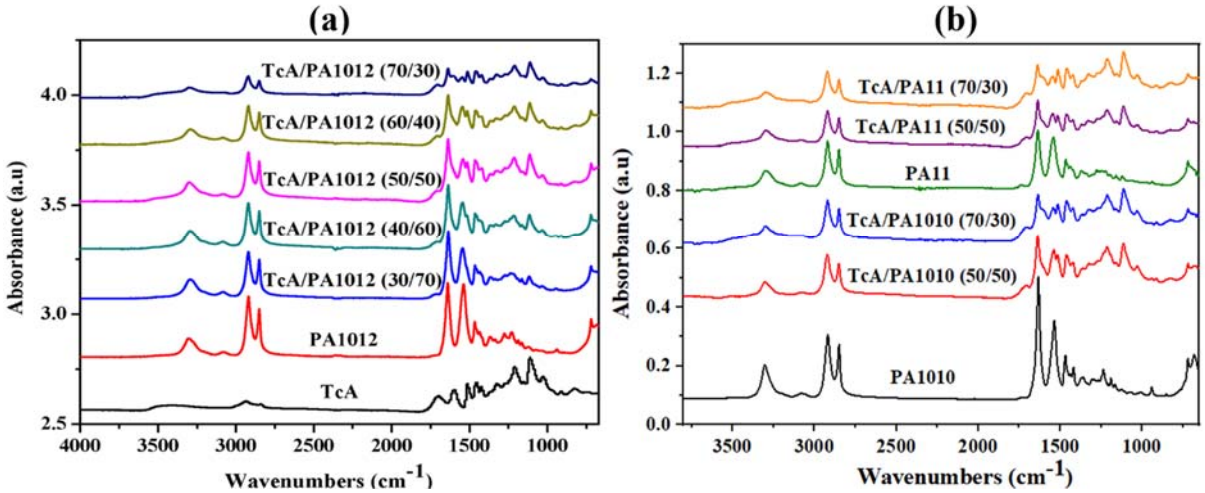

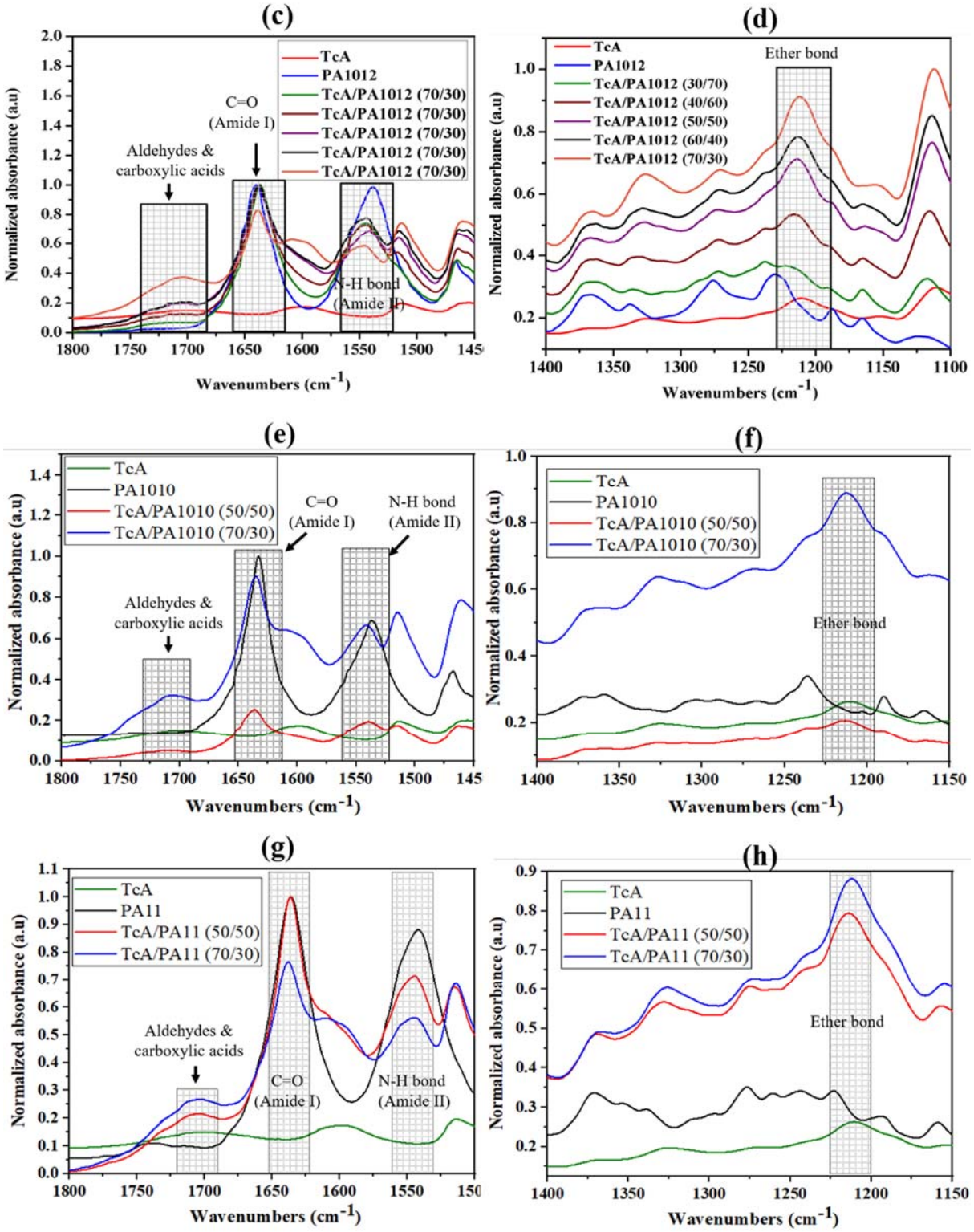

Figure 1. FTIR spectra of (a) and (b) TcA, PA11, PA1010, PA1012 and their blends; (c) and (d) TcA, PA1012 and their blends; (e) and (f); TcA, PA1010 and their blends; (g) and (h) TcA, PA11 and their blends normalised against the absorbance from 1800-1450 cm^{-1} and 1400-1150 cm^{-1}.

Table 2. Characteristic FTIR peaks of TcA, different bio-polyamides and TcA/PA blends

Samples	Lignin (TcA) (aldehydes and carboxlic acid), cm^{-1}	Lignin (TcA) (ether bond), cm^{-1}	Polyamide C=O bond (amide I), cm^{-1}	Polyamide N-H bond (amide II) cm^{-1}
TcA	1698	1210	-	-
PA1012	-	-	1641	1538
TcA/PA1012 (50/50)	1704	1214	1637	1541
TcA/PA1012 (70/30)	1704	1213	1639	1545
PA1010	-	-	1633	1536
TcA/PA1010 (50/50)	1707	1214	1637	1539
TcA/PA11 (70/30)	1708	1213	1635	1541
PA11	-	-	1636	1542
TcA/PA11 (50/50)	1702	1214	1637	1544
TcA/PA11 (70/30)	1706	1213	1638	1544

From these results while some interaction between TcA and all three polyamides can be observed because of the slight shifts identified above, the extent of interaction could not be quantified or distinguished between different TcA/PA blend types, however. This is because non-hydrogen-bonded N-H (3445 cm^{-1}) and C=O (1675 cm^{-1}) peaks of each of the polyamides are overlapping with blended lignin functionalities. As a result, the quantification of hydrogen bonding percentages in these blends may not be easily calculated. Therefore, the interactions could be confirmed only by observing the characteristic peak shifts in the resulting blends FTIR spectra compared to their parent components.

3.2 Differential Scanning Calorimetry Analysis

The first heating cycle of TcA reveals a broad endothermic peak stretching through the glassy region (Figure 2(a)). The broad endothermic peak could also be partly due to water release. During second heating, a clear T_g value can be noticed at 103ºC for the TcA (Figure 2(a)). In order to observe the effect of TcA on the melting and crystallization behaviour of polyamides, second heating (first heating cycles were used to remove the thermal history of the samples) and first cooling cycles of polyamide and TcA/PA blends are shown in Figures

2(b) – (e). The second order transition of the polyamides and TcA/PA blends was expected to be above 55ºC, however, it was not apparent in the DSC heating traces. All the polyamides (PA1010, PA11 and PA1012) exhibit melting points at about 190ºC with a crystallization temperature above 150ºC (Figures 2(b-e)). In the second heating cycle, all the neat polyamides showed bimodal melting points between 180 to 200ºC. The bimodal melting points may be directly associated with the two different types of crystals formation during cooling. The less prefect crystals melt at lower temperatures while the more perfect crystals melt at higher temperatures [34,43,44]. The melting point values (T_m) of all the polyamides gradually reduced with increasing TcA content (Table 3). For a similar blend ratio (e.g. 50/50), the order of reduction for different PA types is as: PA11 > PA1012 > PA1010. The T_m of the PA1012 and PA11 was reduced by about 20ºC in the presence of 70 wt.% TcA. The reduced T_m value is in good agreement with parallel reductions in crystallinity and melting enthalpy (ΔH_m) (Table 3 and Figure 2(f)). The reduced T_m, ΔH_m and crystallinity values of the blends are attributed to the thermodynamic interaction between the TcA and polyamide. No melting peak could be observed in the TcA/PA1010 (70/30) blend, which could be due to the hindrance of crystallization of the PA1010 in the presence of 70 wt.% TcA. A similar observation has been found in lignin/poly(ethylene oxide) blends with higher lignin content [28]. Another possible reason for the observed disappearance of the TcA/PA1010 (70/30) blend melting endotherm is the fast, simultaneous onset of crosslinking at higher temperatures because the DSC heating cycle was performed up to 250ºC followed by cooling and heating to 250ºC. The crystallization temperature (T_c) of the TcA/PA blends was significantly lower compared to their corresponding neat polyamide values (Figures 2(d) and (e)), the order for 50/50 blends being PA11 > PA1010 > PA1012 (Table 3). The crystallisation exotherm has disappeared in the TcA/PA1012 (70/30), TcA/PA1010 (60/40), TcA/PA1010 (70/30) and TcA/PA11 (70/30) blends reflecting the respective diminution in intensity absence of melting

endotherms. Sallem-Idrissi *et al.* [45] have reported similar observations in lignin/PA11 blends. The reduced crystallinities of the TcA/PA blends are most likely due to the interaction between the components of the blends, which leads to enlarged supramolecular structures which thus hinder the formation of large polyamide crystalline regions [45,46]. Due to the slow crystallization rate of the TcA/PA blends, a cold crystallization temperature (T_{cc}) was observed when the TcA content was 50 wt.% or higher (Table 3). For example, the TcA/PA11 blend with ≥50 wt.% TcA, the TcA/PA1010 blend with ≥60 wt.% TcA and the TcA/PA1012 blend with 70 wt.% TcA showed T_{cc} values between 110-140ºC (Table 3). The observed T_{cc} behaviour again suggests the influence of TcA on the polyamide crystallization process.

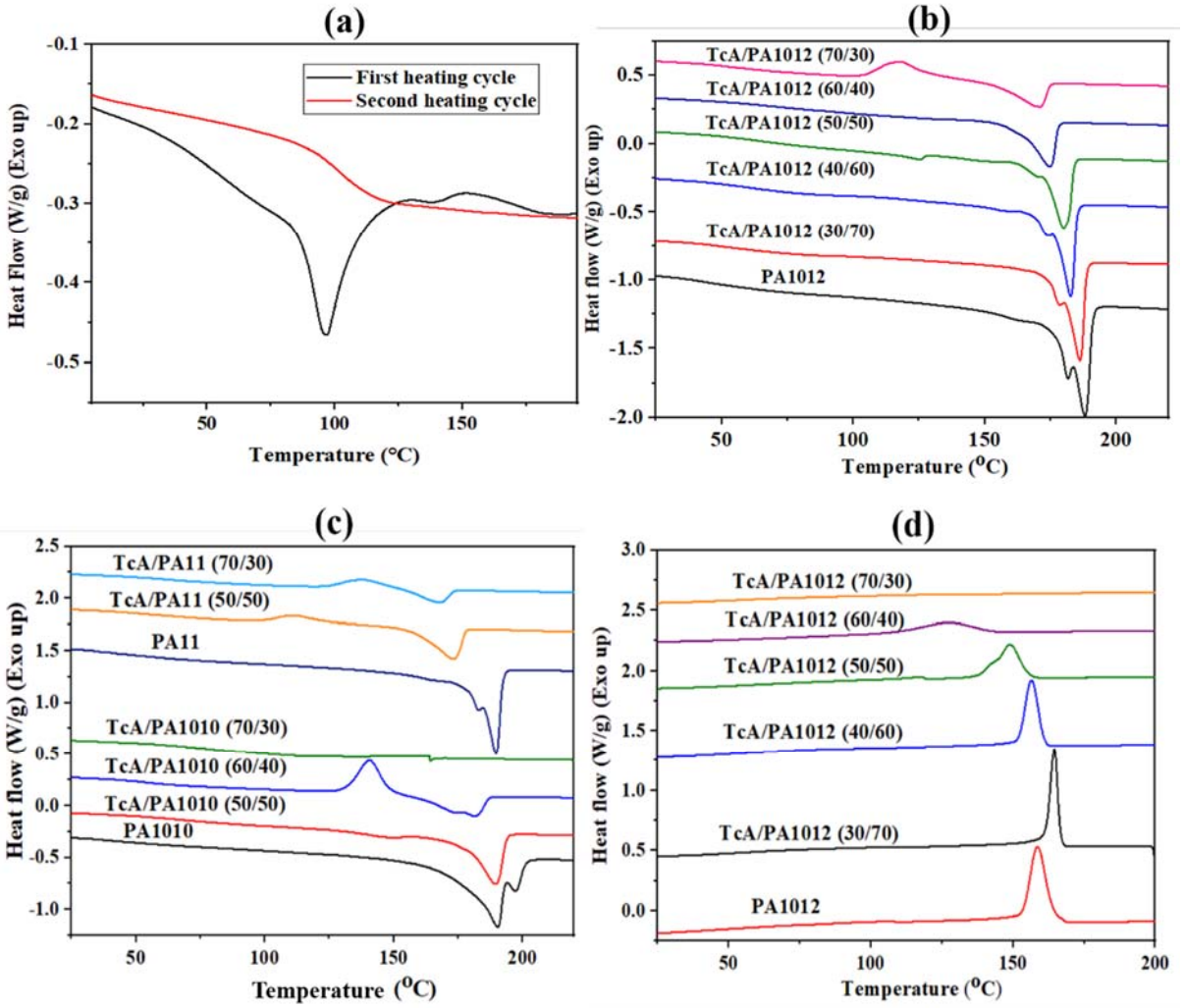

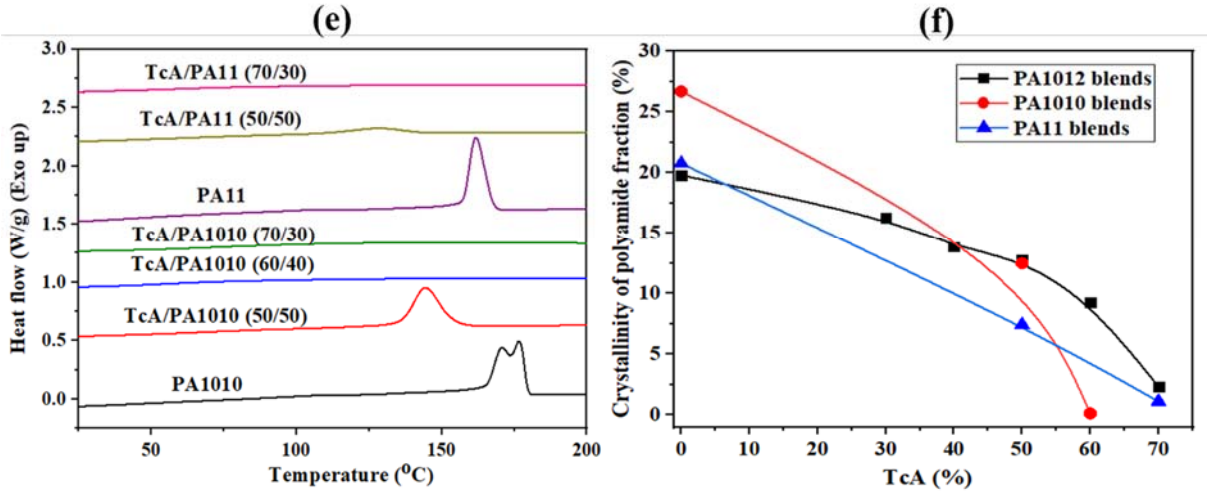

Figure 2. (a) DSC traces of TcA; (b) and (c) second heating scans of different bio-polyamides and TcA/PA blends; (d) and (e) first cooling scan of different bio-polyamides and TcA/PA blends and (f) crystallinity percentages in the TcA/PA blends.

Table 3. Summary of DSC analyses of TcA, different bio-polyamides and TcA/PA blends

Samples	T_m (°C)		ΔH_m (J/g)		T_c (°C)		T_{cc} (°C)	ΔH_{cc} (J/g)	T_g (measured by DMA)* (°C)
	T_m	[a]Red. w.r.t. PA	ΔH_m	[a]Red. w.r.t. PA	T_c	[a]Red. w.r.t. PA			
TcA	x	-	X	-	x	-	X	x	108
PA1012	190	-	41.44	-	162	-	X	x	60
TcA/PA1012 (30/70)	186	4	34.08	7.36	165	+3	X	x	70,111
TcA/PA1012 (40/60)	183	7	29.00	12.44	157	5	X	x	68,112
TcA/PA1012 (50/50)	180	10	26.64	14.8	149	13	X	x	69,118
TcA/PA1012 (60/40)	175	15	19.37	22.07	127	35	X	x	67,123
TcA/PA1012 (70/30)	171	19	12.48	28.96	-	-	117	7.57	85,127
PA1010	190	-	65.12	-	177	-	X	x	57
TcA/PA1010 (50/50)	190	0	30.51	34.61	144	33	X	x	85,110
TcA/PA1010 (60/40)	182	8	19.14	45.98	-	-	141	8.80	92
TcA/PA1010 (70/30)	x	x	X	-	x	-	X	x	100, 132
PA11	188	-	47.01	-	159	-	X	x	58

TcA/PA11 (50/50)	173	15	21.91	25.1	123	36	112	5.07	81, 134
TcA/PA11 (70/30)	167	21	8.47	38.54	x	-	138	5.93	90, 129

Note: x = Not observed
'-' = Not expected/applicable
[a] = Reduction with respect to respective polyamide value

3.3 Dynamic Mechanical Analysis

Since the glass transition temperatures could not be observed by DSC, these were obtained by DMA and the results are given in Table 3. Similarly, other researchers have also used DMA to detect the T_g value of the polyamides because of their inability to observe them using DSC [32]. The T_g values of polyamide and TcA are between 57-60ºC and about 108ºC, respectively (Table 3). All the blend samples showed two T_g values which correspond to the polyamide and TcA. These separate values suggest that the polyamide and TcA were not miscible at the molecular level (Figure 3). However, the T_g value of each polyamide and TcA in all the blends was higher compared to their respective neat sample T_g values. Such an increased T_g value of the blended component was mainly due to the enhanced interaction between the blended component. Among the produced blends, TcA showed a maximum T_g increase in the TcA/PA11 blend (+23, +26 ºC in 50/50 blend), which indicates better compatibility compared to TcA/PA1010 (+30, +2 ºC) and PA1012 (+9, +10 ºC). Evidence of enhanced compatibility was further supported following morphological analysis as shown in the section below.

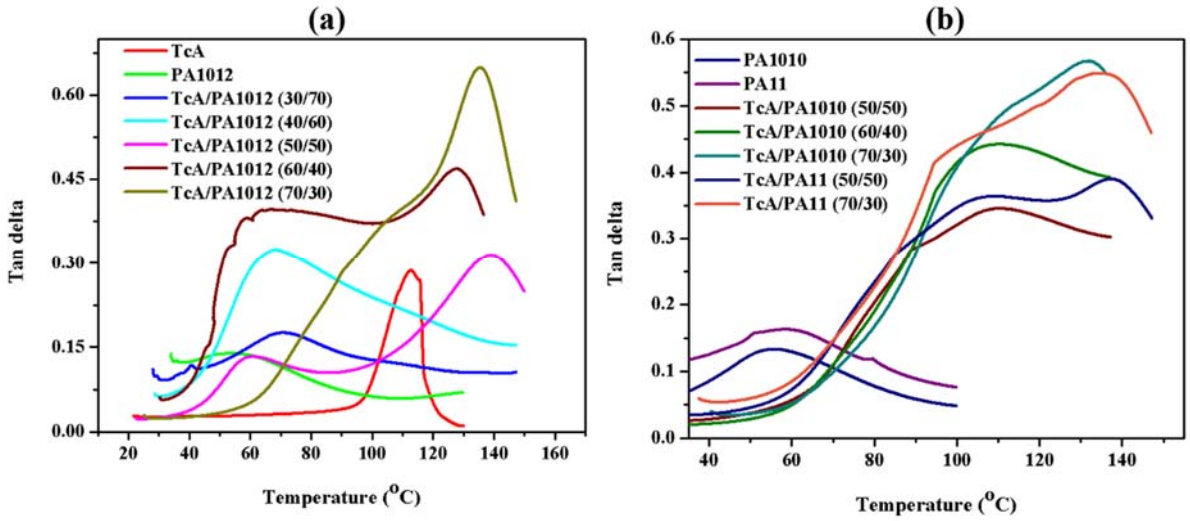

Figure 3. DMA analysis (a) TcA, PA1012, and their blends; (b) TcA/PA1010 and TcA/PA11 blends

3.3 Thermogravimetric Analysis

The TGA profiles under nitrogen of TcA and each different polyamide are shown in Figure 4. The onset of thermal degradation temperature (T_{Onset}), taken as temperature at which 5% mass loss occurs, the temperature at which maximum mass loss (T_{Max}) occurs and the residual mass (char) values calculated from these curves are given in Table 4. T_{Onset} value of the TcA is around 259°C with a maximum degradation temperature of around 380°C. It can be seen that the PA1012, PA1010 and PA11 have significantly higher T_{Onset} values compared to TcA. As can be seen from Figure 4, the shapes of the TGA curves of TcA/PA blends are intermediate to those of TcA and the respective PAs (Figure 4(a)), which is expected from a physical blend. A similar observation is noted for T_{Onset} values of blends, which are intermediate values between those for TcA and PAs, the lowest being for TcA/PA11 70/30 (220°C). However, these values are higher than the processing temperature of the blends during melt blending, 190°C max (Table 1), indicating that minimal polymer degradation has occurred during processing.

While chemical interaction between different components of the blends appears to be minimal up to 200ºC, interactions leading to crosslinking at higher temperatures is likely to yield higher residual char formation. Higher char formation is relevant to higher carbon yield for carbon fibre production or lower flammability in case of flame-retardant polymer applications. To observe this possible effect, the calculated mass losses ((mass fraction of TcA × measured mass loss of TcA) + (mass fraction of PA × measured mass loss of PA) at each temperature subtracted from the respective experimental mass losses are plotted in Figure 5 as mass differential versus temperature curves. Any negative or positive deviations indicate negative or positive interactions between the components. As can be seen from Figure 5, for TcA/PA1012 and TcA/PA1010 blends over the range 350-475ºC and for TcA/PA11 blends between ~ 350-440ºC there is more than expected mass loss, indicating that one component sensitizes the thermal decomposition of the other component. Such a behaviour has previously been seen in our work on different blends and polymers containing additives [47,48]. However, above 470ºC more than expected char is formed in each blend. The absolute values of the char residual values at 880ºC are given in Table 4 with that of the TcA being 37% at 880ºC and those of the PAs < 1% reflecting their respective residual carbon contents. As expected, the higher the lignin content in the blend the higher is char residue with actual values being higher than calculated values. It can be seen that all the blends with 70 wt.% TcA showed more than 30% char residues at 880ºC (Figure 5b), considerably higher than respective calculated values suggesting that these observed high contents of char residue could be useful indicators of blend potential as precursor fibres for carbon fibre production [49]. The char forming tendency of different blends can be ranked as: TcA/PA11 > TcA/PA1010 ≈ TcA/PA1012.

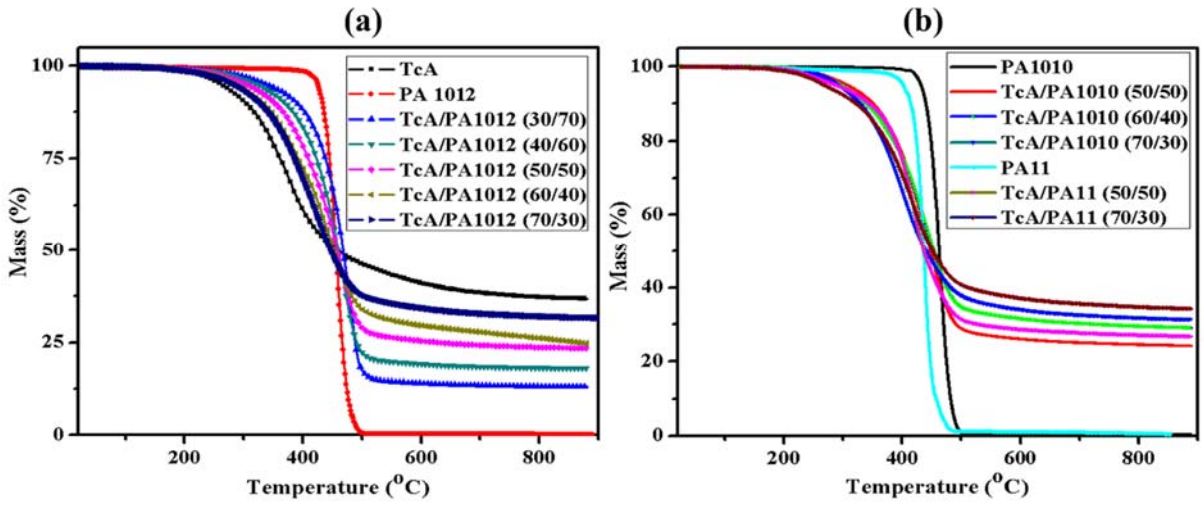

Figure 4. TGA responses of (a) TcA and blends with PA1012 and (b) TcA blends with PA11 and PA1010 under nitrogen

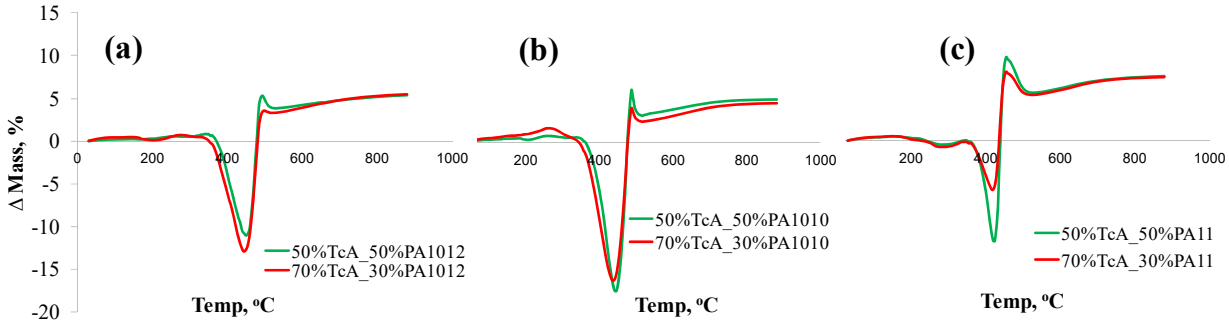

Figure 5. Mass differential curves as functions of temperature for TcA/PA1012, TcA/PA1010 and TcA/PA11 blends in nitrogen.

Table 4. Summary of TGA analysis (under nitrogen) of TcA, different bio-polyamides and TcA/PA blends

Samples	T_{Onset} (°C)	T_{Max} (°C)	Char yield at 880°C (%)
TcA	259	380	37.3
PA1012	429	478	0.1
TcA/PA1012 (30/70)	336	484	13.3 (11.2)
TcA/PA1012 (40/60)	320	468	18.1 (14.9)
TcA/PA1012 (50/50)	302	465	23.7 (18.7)
TcA/PA1012 (60/40)	281	443	26.1 (22.4)

TcA/PA1012 (70/30)	283	423	32.0 (26.1)
PA1010	433	465	0.4
TcA/PA1010 (50/50)	298	450	24.5 (18.9)
TcA/PA1010 (60/40)	293	442	29.4 (22.5)
TcA/PA1010 (70/30)	287	403	31.8 (26.2)
PA11	397	438	0.6
TcA/PA11 (50/50)	282	421	27.1 (19.0)
TcA/PA11 (70/30)	264	420	34.7 (26.3)

Note: The values in the parentheses for the blends are the calculated weighted average mass residues from those of individual components

3.5 Rheological Properties

Figures 6 and 7 show the complex viscosity, storage modulus and loss modulus curves of the neat TcA, polyamides and their blends as a function of frequency (from higher to lower). The TcA, PA1012 and PA1010 showed typical shear-thinning flow behaviour whereas PA11 viscosity is almost independent of shear rate within the tested frequencies as shown in Figure 6(a). Therefore, PA11 flow behaviour can be considered as Newtonian. Upon addition of the TcA (50 wt.%), the viscosity of the respective polyamide was considerably reduced because of the lower viscosity of the TcA (Figure 6(b)). The reduced viscosities of the TcA/PA blends could be an advantage for melt spinning of these blends into fibres, however for the latter good melt strength is also required. It has been observed (Figure 6(a)) that the TcA can undergo rapid crosslinking at elevated temperatures because of its reactive structure [3,4]. As a result, the TcA/PA1012 (50/50) and TcA/PA1010 (50/50) blends showed a sharp viscosity increase at the lower frequency regions, whereas TcA/PA11 (50/50) blend did not show this feature as clearly (Figure 6(b)). The observed viscosity increases in these blends at lower frequencies (<0.4 rad/s) could be due to the slow intra- and inter-molecular rearrangements which can change the molecular size distribution and molecular polarities [3]. Unlike PA1012 and PA1010, the lower viscosity of PA11 might have accelerated the chemical reactivity of the TcA within the time scale of experiment. Therefore, the TcA/PA11 (50/50) blend showed a viscosity curve more similar to that for TcA. The intra- and inter-molecular reactivity of the TcA could be a

predominant effect when the TcA/PA blends were prepared with 70 wt.% TcA, regardless of the polyamide. Consequently, the viscosity increases in the 70 wt.% TcA blends were similar to that for TcA within the tested frequency range.

Figure 7 shows the viscoelastic properties (storage modulus (G') and loss modulus (G")) of the samples. G' and G" represent the ability of a material to store energy during deformation and the amount of energy dissipated in the viscous portion, respectively. At low frequency, the G" value was lower than G' for PA1010 (Figure 7(a)), indicating a low viscous response in the molten state [15]. However, TcA exhibits higher G' than G" values at lower frequencies (<10 rad/s), which indicates that the TcA is behaving like a stiff material. As expected, the viscoelastic properties of the polyamides reduced after the addition of TcA (see Figure 6) in terms of the observed viscosity reduction in the blends. All the blends (Figures 7 (b) and (c)) behave predominantly as fluids with each having a higher G" than the G' at above 1 rad/s, although the stiffening effect by crosslinking becomes more apparent at lower frequencies for prolonged thermo-rheological shear exposure [15]. The crosslinking rate of the blends can be further confirmed by noting the angular frequency crossover points of the respective G" and G' versus ω curves (Figures 7 (b) and (c)). For example, the TcA trends had a crossover point at a higher frequency (*i.e.* 12.5 rad/s) while all the blends showed crossover points < 4 rad/s. More specifically, TcA/PA1012 (50/50) and TcA/PA1010 (50/50) blend trends had crossover points of 0.3 and 0.4 rad/s respectively. However, the crossover points of the TcA/PA1012 (70/30) and TcA/PA1010 (70/30) blends were slightly higher compared to their corresponding blends with 50 wt.% TcA (Figures 7 (b) and (c)). The observed higher ω values at the crossover points in the 70 wt.% TcA blends could be the result of the higher TcA content in the blend leading to faster interchange reactions between the molecules through more contact between the molecules. Furthermore, the TcA/PA11 (70/30) blend showed a faster onset of crosslinking ω value (2.5 rad/s) compared to those for the TcA/PA1012 and TcA/PA1010 blends. Such a

faster onset of crosslinking point could be due to the better dispersion of the TcA in the lower viscosity PA11 phase, thereby enhancing the interchange interactions between the TcA molecules, the order being TcA/PA11 > TcA/PA1010 ≈ TcA/PA1012. Overall, the TcA/PA blends' rheological properties suggest that these blends should be melt processable using a short residence time to avoid or minimise possible crosslinking during processing.

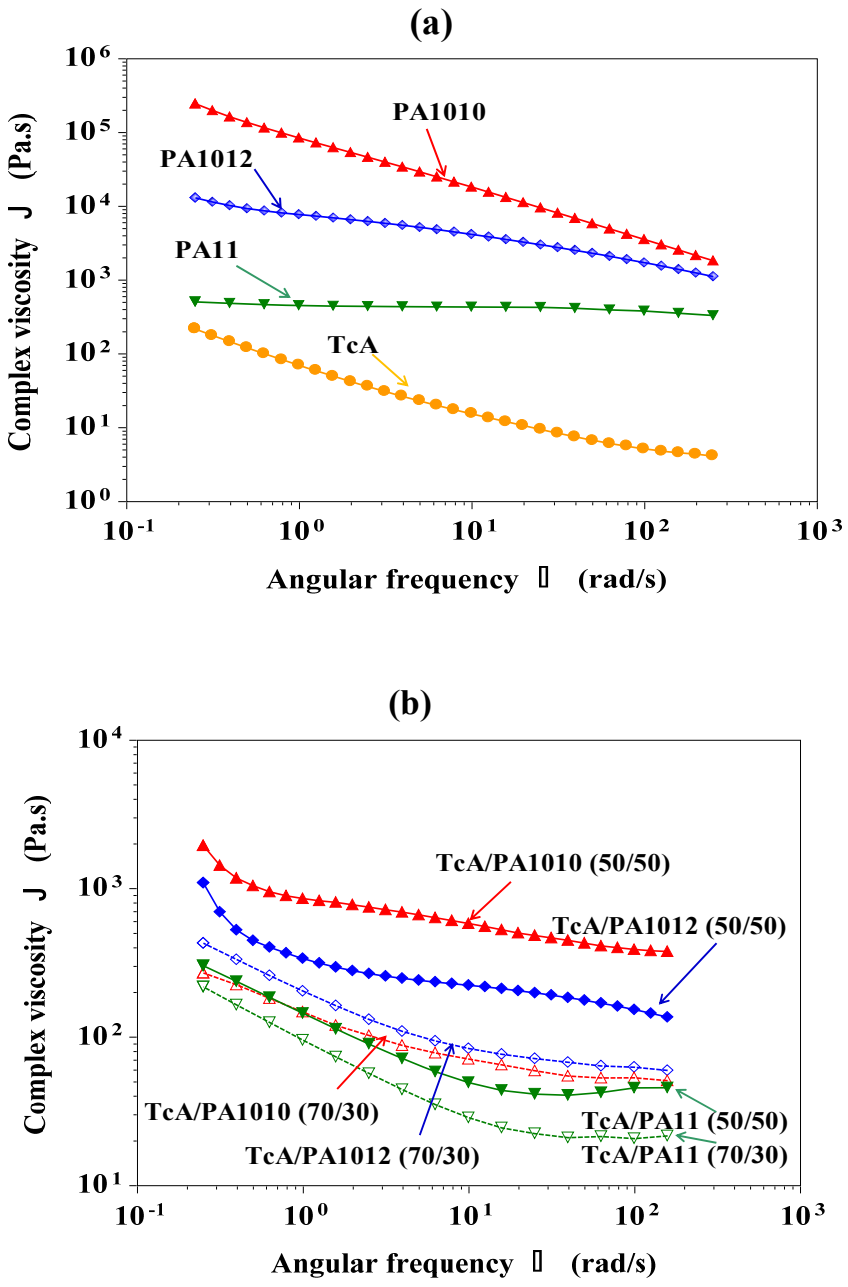

Figure 6. Complex viscosity versus angular frequency of (a) neat TcA, bio-polyamides and (b) TcA/PA blends

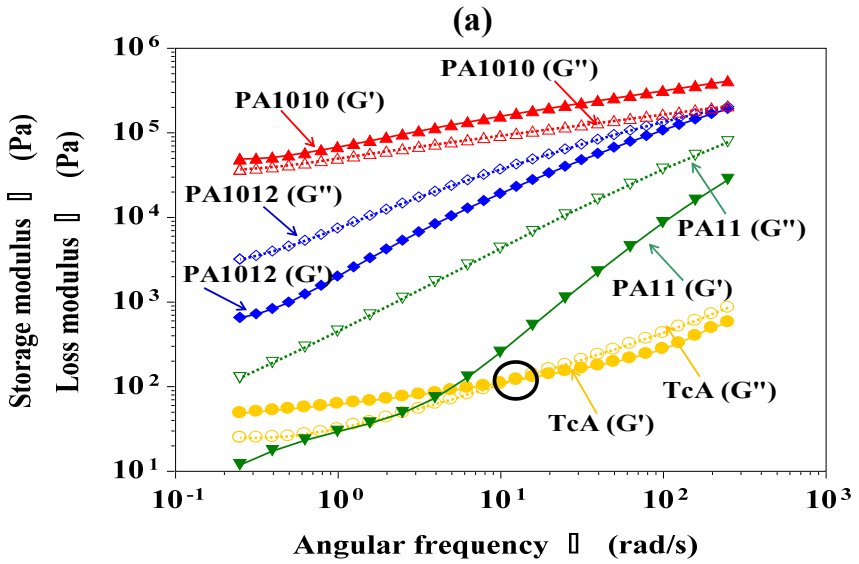
(a)
PA1010 (G'')
PA1010 (G')
PA1012 (G'')
PA1012 (G')
PA11 (G'')
PA11 (G')
TcA (G'')
TcA (G')
Storage modulus (Pa)
Loss modulus (Pa)
Angular frequency (rad/s)

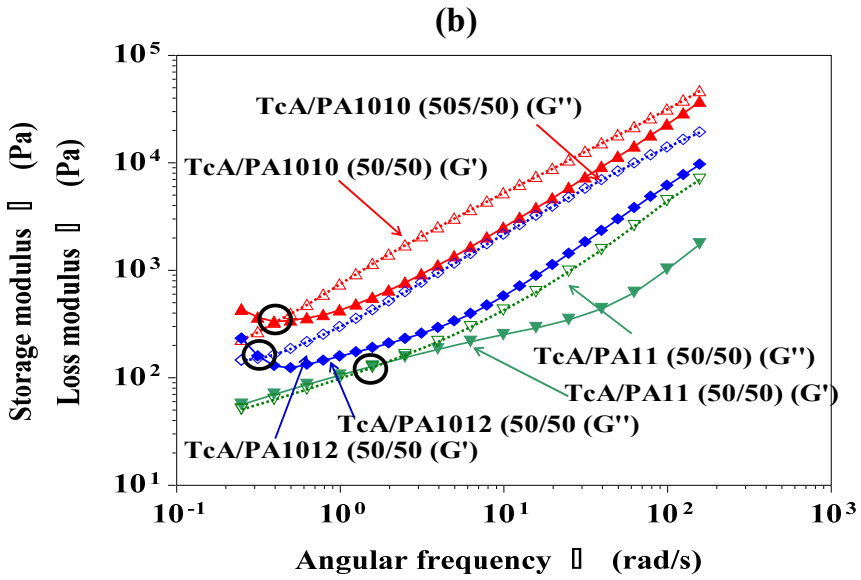
(b)
TcA/PA1010 (505/50) (G'')
TcA/PA1010 (50/50) (G')
TcA/PA11 (50/50) (G'')
TcA/PA11 (50/50) (G')
TcA/PA1012 (50/50 (G'')
TcA/PA1012 (50/50 (G')
Storage modulus (Pa)
Loss modulus (Pa)
Angular frequency (rad/s)

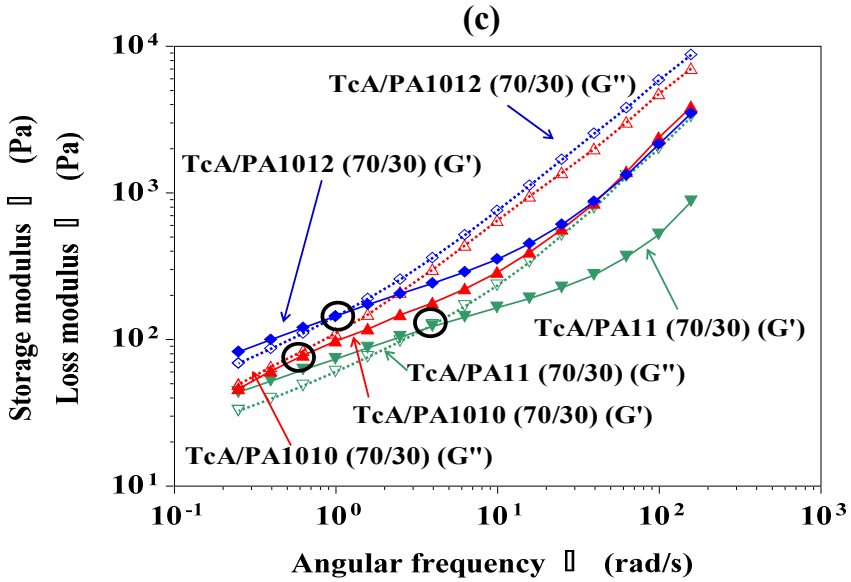
(c)
TcA/PA1012 (70/30) (G'')
TcA/PA1012 (70/30) (G')
TcA/PA11 (70/30) (G')
TcA/PA11 (70/30) (G'')
TcA/PA1010 (70/30) (G')
TcA/PA1010 (70/30) (G'')
Storage modulus (Pa)
Loss modulus (Pa)
Angular frequency (rad/s)

Figure 7. Storage modulus (G') and loss modulus (G'') versus angular frequency plots for (a) neat TcA, bio-polyamides and (b,c) TcA/PA blends (crossover points are circled)

3.6 Scanning Electron Microscopic Analysis

Scanning electron microscopy images of the TcA/PA blends are shown in Figure 8. Regardless of the polyamide, the morphology of the blends showed heterogeneous morphology with dispersed TcA in the polyamide (Figures 8(a) – (f)). The sizes of the lignin domains depend very much on the interaction with polyamide as previously stated. The observed heterogenous morphologies of the TcA/PA blends were most likely due to the polar nature of TcA with its large number of functional groups, which can from strong self-interactions. Furthermore, the lack of phase inversion and co-continuous morphology formation at higher TcA content (70 wt.%) suggests strong self-interactions within the TcA molecules, which prevents their facile dispersion. The SEM micrographs can offer only qualitative information of structure and particle size. However, the average sizes dispersed lignin domains in each blend were determined quantitatively by image J analysis, and each number average is plotted against the composition of the respective blend in Figure 8(g). The final size of the dispersed domain depends on thermodynamic and kinetic factors, *i.e.* on interactions/interfacial tension and the shear forces prevailing during mixing [50]. The size of the original solid TcA domain was >15 μm which reduced to below 1μm in all the blends containing 50 wt.% TcA during homogenization (Figure 8(g)). The extent of TcA domain size reduction most likely depends on the interaction of the two components. However, the dispersed TcA domain size was significantly increased in the PA1012 and PA1010 blends containing 70 wt.% TcA, even after two step processing. This increase in domain size with increasing lignin content seems to be intuitively correct because larger particle formation would be generally expected at larger lignin concentrations. On the other hand, the TcA/PA11 blend with 70 wt.% TcA did not show

much difference in the TcA domain size compared to the 50 wt.% blend (Figure 8(g)). This could be due to the lower viscosity (a kinetic factor) of the PA11 which played a role in reducing the TcA domain size in these blends as well as the greater TcA/PA interaction suggested by the DSC and DMA results above. These results also suggest that both the thermodynamic (*i.e.* interaction) and the kinetic factors are dominant in the PA1010 and PA1012 blends and changing shear by two step processing did not reduce the TcA domain sizes. Our results show good agreement with domain size effects reported in ionomer/lignin and plasticized lignin/poly(vinyl chloride-co-vinyl acetate) blends [8,50,51].

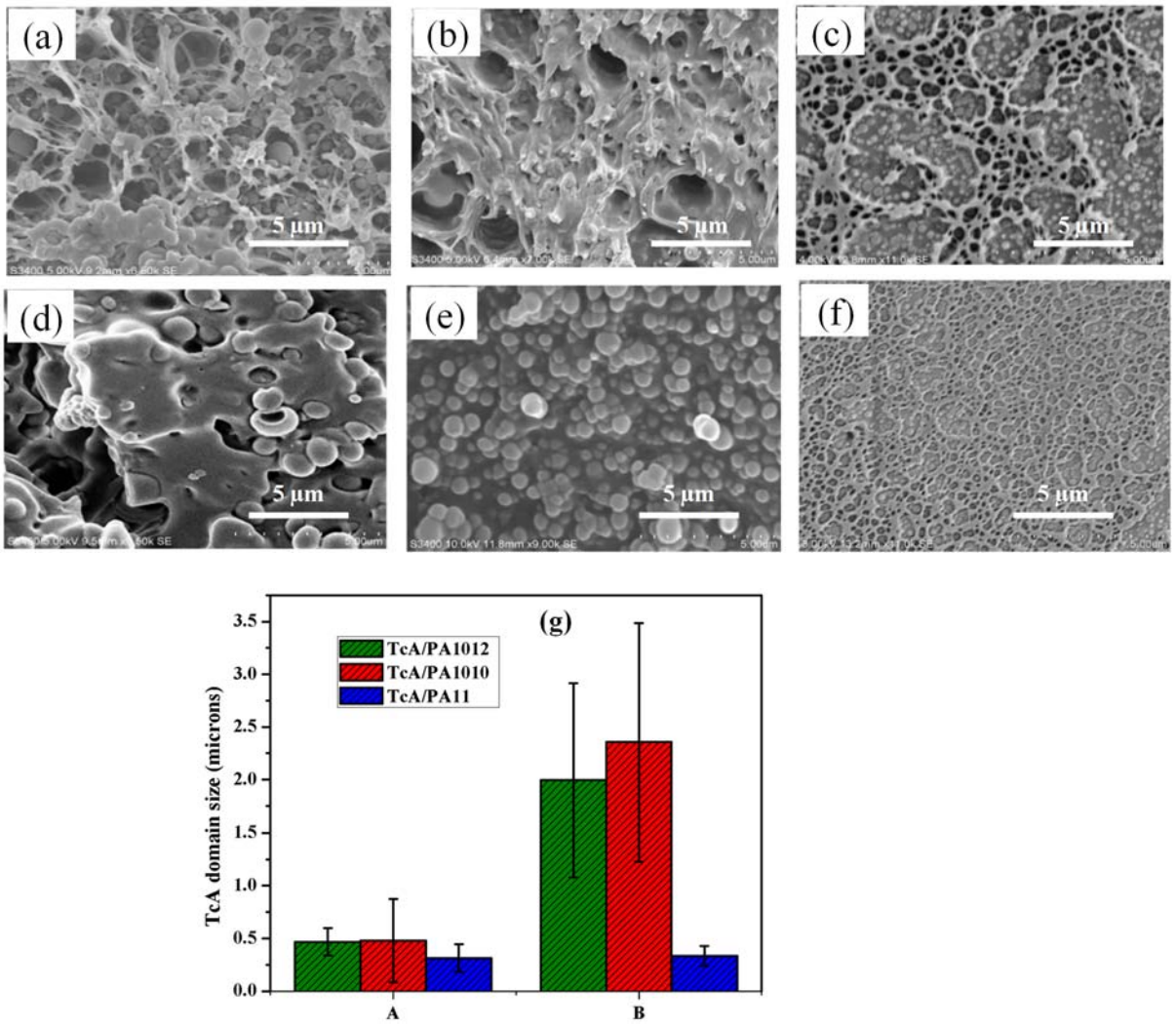

Figure 8. SEM images of the TcA/PA blends: (a) TcA/PA1010 (50/50), (b) TcA/PA1012 (50/50), (c) TcA/PA11 (50/50), (d) TcA/PA1010 (70/30), (e) TcA/PA1012 (70/30), (f)

TcA/PA11 (70/30) and (g) TcA domain sizes in the different blends (A: TcA/PA (50/50) and B: TcA/PA (70/30))

From these results the dispersibility of TcA in polyamide in respective 50/50 blends can be ranked as PA11 > PA1010 ≈ PA1012. In 70/30 blends, while TcA in PA11 is dispersed well, both PA1010 and PA1012 are not.

3.7 Thermodynamics of the miscibility and compatibility

As mentioned in Section 2.4, the interaction between the blended polymers can be analysed in terms of Gibb's free energy, $\Delta G_m = \Delta H_m - T\Delta S_m$ (Eqn. 2) and a negative ΔG_m must be observed in the polymer blends if they are to achieve miscibility or intimate mixing. Since both lignin and the bio-polyamides used have high molecular weights, ΔS_m is negligible in lignin and polyamide blend systems [35]. ΔH_m was calculated by using Eqns. 3 and 4 to identify the miscibility of the lignin/polyamide blends. The solubility parameter (δ) values of the lignin and polyamides were obtained from the molecular weight of the respective repeat unit shown in Figure 9 (M), density (ρ), and group molar attraction constants (G_m).The G_m values of the polyamides and TcA, taken from reference [52], where Hoy calculated these values for different functional groups, are given in Table 5. Using these G_m values, densities (lignin: 1.33 g/cm^3, PA1012: 1.03 g/cm^3, PA1010: 1.05 g/cm^3 and PA11: 1.04 g/cm^3) [32,53,54] and molecular weights of the mer units (lignin: 648.70 g/mol, PA1012: 366.58 g/mol, PA1010: 338.53 g/mol and PA11: 183.29 g/mol), solubility parameters (δ) values were calculated using Eqn. 4). The δ values of TcA and polyamides together with ΔG_m values (Eqn. 2) of the TcA/PA blends are given in Table 6. The solubility parameter values of all the polyamides are nearly the same, whereas TcA had a slightly higher solubility parameter value (21.56 J$^{1/2}$ cm$^{3/2}$). Among the prepared blends, the TcA/PA11 blends generally showed a lower ΔG_m value

compared to other blends (Table 6), which was especially notable for the TcA/PA11 (70/30) blend with the lowest ΔG_m value (0.115 J/g m^3). Again, this suggests that the TcA/PA11 blend is more compatible, with the decreasing order being TcA/PA11 > TcA/PA1010 > TcA/PA1012. This trend is consistent with those interpreted from the experimental results using different techniques.

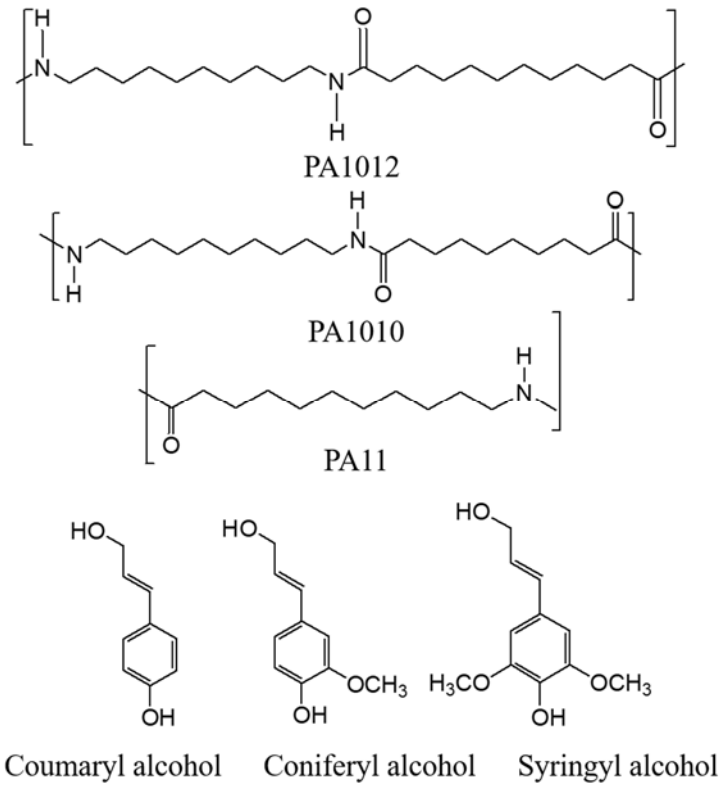

Figure 9. Repeating units of bio-polyamides and TcA considered for molar group attraction calculation

Table 5. Group molar attraction constant, *Gm*, for TcA and bio-polyamides [52]

Groups	Number of groups	Hoy ($J^{1/2}$ $cm^{3/2}$ mol^{-1})	
		G_m	$G_{m(total)}$
PA11			
-(C=O)-	2	538	1076
$-CH_2-$	20	269	5380
-NH	2	368	736
PA1010			
-(C=O)-	2	538	1076
$-CH_2-$	18	269	4842
-NH	2	368	736

PA1012			
-(C=O)-	1	538	538
-CH_2-	10	269	2690
-NH	1	368	368
TcA			
Aromatic CH	12	241	2892
Aromatic C	6	201	1206
Aromatic (meta substation)	3	13.5	40.5
Aromatic (para substation)	3	83	249
-O-	6	235	1410
-OCH_3	3	236	708
=CH-	3	249	747
-CH_2-	3	269	807

Note: $G_{m(total)}$ is sum of the molar group attraction (G_m) of individual functional group

Table 6. Solubility parameter value of TcA and bio-polyamides as well as Gibbs free energy of the TcA/PA blends.

Samples	Group molar attraction constant (G_m) ($J^{1/2}$ $cm^{3/2}$ mol^{-1})	Solubility parameter (δ) $J^{1/2}$ $cm^{3/2}$	Gibbs free energy (ΔG_m) (J/g m^3)
Lignin (TcA)	8059.5	21.57	-
PA1012	7192	20.24	-
PA1010	6654	20.67	-
PA11	3596	20.83	
TcA/PA1012 (50/50)	-	-	0.44
TcA/PA1012 (70/30)	-	-	0.37
TcA/PA1010 (50/50)	-	-	0.20
TcA/PA1010 (70/30)	-	-	0.17
TcA/PA11 (50/50)	-	-	0.14
TcA/PA11 (70/30)	-	-	0.11

4 Conclusions

This study has shown that an organosolv hardwood lignin (TcA) can be successfully blended with different bio-based polyamides, PA1012, PA1010 and PA11, with the maximum processable lignin/PA blend ratio being 70/30 wt.%. The TcA/PA blends showed varying degrees of compatibility in the decreasing order TcA/PA11 > TcA/PA1010 > TcA/PA1012,

indicated by FTIR, morphological, DSC, DMA and rheological analyses. This compatibility order was also supported by theoretically calculating the interaction between the components of the blends using Gibbs free energy equation. It was also observed that the presence of lignin in the blends reduces the crystallinity of polyamide and the extent of reduction depends on the polyamide type. From rheological studies it was seen that the addition of TcA reduced the viscosities of the blends compared to that of the respective polyamide, which indicates that the melt spinning of these blends into fibres will be possible. Furthermore, onset points of crosslinking could be determined for each blend. The enhanced charring tendency of the blends, caused by crosslinking between TcA and respective PA components suggest that the fibres produced from these blends have a potential to be used as precursors for carbon fibre production. This aspect will be explored in our future publications.

Acknowledgements

The authors acknowledge the funding received from the BioBased Industries Joint Undertaking under the European Union's Horizon 2020 research and innovation programme grant agreement no. 720707.

References

[1] R. Muthuraj, T. Mekonnen, Recent progress in carbon dioxide (CO2) as feedstock for sustainable materials development: Co-polymers and polymer blends, Polymer . 145 (2018) 348–373. doi:https://doi.org/10.1016/j.polymer.2018.04.078.

[2] R. Muthuraj, M. Misra, A.K. Mohanty, Biodegradable compatibilized polymer blends for packaging applications: A literature review, J. Appl. Polym. Sci. 135 (2018) 45726. doi:10.1002/app.45726.

[3] Q. Sun, R. Khunsupat, K. Akato, J. Tao, N. Labbe, N.C. Gallego, J.J. Bozell, T.G. Rials, G.A. Tuskan, T.J. Tschaplinski, A.K. Naskar, Y. Pu, A.J. Ragauskas, A study of poplar organosolv lignin after melt rheology treatment as carbon fiber precursors, Green Chem. 18 (2016) 5015–5024. doi:10.1039/C6GC00977H.

[4] M. Culebras, M.J. Sanchis, A. Beaucamp, M. Carsí, B.K. Kandola, A.R. Horrocks, G. Panzetti, C. Birkinshaw, M.N. Collins, Understanding the thermal and dielectric response of organosolv and modified kraft lignin as a carbon fibre precursor, Green Chem. 20 (2018) 4461–4472. doi:10.1039/C8GC01577E.

[5] R. Muthuraj, T. Mekonnen, Carbon Dioxide–Derived Poly (propylene carbonate) as a Matrix for Composites and Nanocomposites: Performances and Applications, Macromol. Mater. Eng. (2018) 1800366. https://doi.org/10.1002/mame.201800366

[6] D. Kun, B. Pukánszky, Polymer/lignin blends: Interactions, properties, applications, Eur. Polym. J. 93 (2017) 618–641.

[7] H. Zhu, W. Luo, P.N. Ciesielski, Z. Fang, J.Y. Zhu, G. Henriksson, M.E. Himmel, L. Hu, Wood-Derived Materials for Green Electronics, Biological Devices, and Energy Applications, Chem. Rev. 116 (2016) 9305–9374. doi:10.1021/acs.chemrev.6b00225.

[8] B. Podolyák, D. Kun, K. Renner, B. Pukánszky, Hydrogen bonding interactions in poly (ethylene-co-vinyl alcohol)/lignin blends, Int. J. Biol. Macromol. 107 (2017) 1203–1211.

[9] G. Markovic, P.M. Visakh, Polymer blends: State of art, In: P.M. Visakh, G. Markovic, D. Pasquini (Eds.), Recent Developments in Polymer Macro, Micro and Nano Blends: Preparation and Characterisation, Woodhead Publishing, Cambridge, UK, 2016, pp. 1-15.

[10] R. Pucciariello, V. Villani, C. Bonini, M. D'Auria, T. Vetere, Physical properties of

straw lignin-based polymer blends, Polymer . 45 (2004) 4159–4169.

[11] R.R.N. Sailaja, M. V Deepthi, Mechanical and thermal properties of compatibilized composites of polyethylene and esterified lignin, Mater. Des. 31 (2010) 4369–4379. doi:https://doi.org/10.1016/j.matdes.2010.03.046.

[12] S. Shankar, J.P. Reddy, J.-W. Rhim, Effect of lignin on water vapor barrier, mechanical, and structural properties of agar/lignin composite films, Int. J. Biol. Macromol. 81 (2015) 267–273.

[13] F. Chen, W. Liu, S.I. Seyed Shahabadi, J. Xu, X. Lu, Sheet-like lignin particles as multifunctional fillers in polypropylene, ACS Sustain. Chem. Eng. 4 (2016) 4997–5004.

[14] J. Tomaszewska, Ł. Klapiszewski, K. Skórczewska, T.J. Szalaty, T. Jesionowski, Advanced organic-inorganic hybrid fillers as functional additives for poly (vinyl chloride), Polimery. 62 (2017) 19–26.

[15] S. Luo, J. Cao, A.G. McDonald, Esterification of industrial lignin and its effect on the resulting poly(3-hydroxybutyrate-co-3-hydroxyvalerate) or polypropylene blends, Ind. Crops Prod. 97 (2017) 281–291. doi:https://doi.org/10.1016/j.indcrop.2016.12.024.

[16] K. Peredo, D. Escobar, J. Vega-Lara, A. Berg, M. Pereira, Thermochemical properties of cellulose acetate blends with acetosolv and sawdust lignin: A comparative study, Int. J. Biol. Macromol. 83 (2016) 403–409.

[17] H. Ali, S. Radhakrishnan, M. B. Kulkarni, Preparation and Characterization of Polybenzoxazine/Plasticized PVC-Based Fumed Silica Composites, In: S. Thottathil, S. Thomas, N. Kalarikkal, D. Rouxel (Eds.), Advanced Polymeric Materials for Sustainability and Innovations, Apple Academic Press Inc, Oakville, Canada, 2018, pp. 75-92

[18] G. Szabó, V. Romhányi, D. Kun, K. Renner, B. Pukánszky, Competitive Interactions

in Aromatic Polymer/Lignosulfonate Blends, ACS Sustain. Chem. Eng. 5 (2017) 410–419. doi:10.1021/acssuschemeng.6b01785.

[19] P. Mousavioun, W.O.S. Doherty, G. George, Thermal stability and miscibility of poly (hydroxybutyrate) and soda lignin blends, Ind. Crops Prod. 32 (2010) 656–661.

[20] P. Mousavioun, P.J. Halley, W.O.S. Doherty, Thermophysical properties and rheology of PHB/lignin blends, Ind. Crops Prod. 50 (2013) 270–275. doi:https://doi.org/10.1016/j.indcrop.2013.07.026.

[21] R. Chen, M.A. Abdelwahab, M. Misra, A.K. Mohanty, Biobased Ternary Blends of Lignin, Poly(Lactic Acid), and Poly(Butylene Adipate-co-Terephthalate): The Effect of Lignin Heterogeneity on Blend Morphology and Compatibility, J. Polym. Environ. 22 (2014) 439–448. doi:10.1007/s10924-014-0704-5.

[22] C. Liu, C. Xiao, H. Liang, Properties and structure of PVP–lignin "blend films," J. Appl. Polym. Sci. 95 (2005) 1405–1411.

[23] G. Cunxiu, C. Donghua, T. Wanjun, L. Changhua, Properties and thermal degradation study of blend films with poly (4-vinylpyridine) and lignin, J. Appl. Polym. Sci. 97 (2005) 1875–1879.

[24] P.C. Rodrigues, M.P. Cantão, P. Janissek, P.C.N. Scarpa, A.L. Mathias, L.P. Ramos, M.A.B. Gomes, Polyaniline/lignin blends: FTIR, MEV and electrochemical characterization, Eur. Polym. J. 38 (2002) 2213–2217.

[25] J.F. Kadla, S. Kubo, Miscibility and Hydrogen Bonding in Blends of Poly(ethylene oxide) and Kraft Lignin, Macromolecules. 36 (2003) 7803–7811. doi:10.1021/ma0348371.

[26] S. Kubo, J.F. Kadla, Poly(Ethylene Oxide)/Organosolv Lignin Blends: Relationship between Thermal Properties, Chemical Structure, and Blend Behavior, Macromolecules. 37 (2004) 6904–6911. doi:10.1021/ma0490552.

[27] J.F. Kadla, S. Kubo, Lignin-based polymer blends: analysis of intermolecular interactions in lignin–synthetic polymer blends, Compos. Part A Appl. Sci. Manuf. 35 (2004) 395–400. doi:http://dx.doi.org/10.1016/j.compositesa.2003.09.019.

[28] S. Kubo, J.F. Kadla, Kraft lignin/poly (ethylene oxide) blends: effect of lignin structure on miscibility and hydrogen bonding, J. Appl. Polym. Sci. 98 (2005) 1437–1444.

[29] G.Z. Zhang, H. Yoshida, T. Kawai, Miscibility of Nylon 66 and Nylon 48 blend evaluated by crystallization dynamics, Thermochim. Acta. 416 (2004) 79–85. doi:https://doi.org/10.1016/j.tca.2003.01.002.

[30] N. Sallem-Idrissi, M. Sclavons, D.P. Debecker, J. Devaux, Miscible raw lignin/nylon 6 blends: Thermal and mechanical performances, J. Appl. Polym. Sci. 133 (2016) 42963.

[31] A. Dasari, Z.-Z. Yu, G.-P. Cai, Y.-W. Mai, Recent developments in the fire retardancy of polymeric materials, Prog. Polym. Sci. 38 (2013) 1357–1387.

[32] L. Quiles-Carrillo, N. Montanes, T. Boronat, R. Balart, S. Torres-Giner, Evaluation of the engineering performance of different bio-based aliphatic homopolyamide tubes prepared by profile extrusion, Polym. Test. 61 (2017) 421–429. doi:http://dx.doi.org/10.1016/j.polymertesting.2017.06.004.

[33] O. Okamba-Diogo, E. Richaud, J. Verdu, F. Fernagut, J. Guilment, B. Fayolle, Investigation of polyamide 11 embrittlement during oxidative degradation, Polymer . 82 (2016) 49–56. doi:https://doi.org/10.1016/j.polymer.2015.11.025.

[34] R. Muthuraj, M. Misra, A.K. Mohanty, Biodegradable Poly(butylene succinate) and Poly(butylene adipate-co-terephthalate) Blends: Reactive Extrusion and Performance Evaluation, J. Polym. Environ. 22 (2014) 336–349. http://dx.doi.org/10.1007/s10924-013-0636-5.

[35] S.L. Ciemniecki, W.G. Glasser, Polymer Blends with Hydroxypropyl Lignin, In: W.-G. Glasser, S. Sarkanen (Eds.), Lignin, American Chemical Society, 1989: pp. 35–452. doi:doi:10.1021/bk-1989-0397.ch035.

[36] S. Sahoo, M.Ö. Seydibeyoğlu, A.K. Mohanty, M. Misra, Characterization of industrial lignins for their utilization in future value added applications, Biomass and Bioenergy. 35 (2011) 4230–4237. doi:http://dx.doi.org/10.1016/j.biombioe.2011.07.009.

[37] S. Kubo, J.F. Kadla, Hydrogen Bonding in Lignin: A Fourier Transform Infrared Model Compound Study, Biomacromolecules. 6 (2005) 2815–2821. doi:10.1021/bm050288q.

[38] M. Porubská, O. Szöllős, A. Kóňová, I. Janigová, M. Jašková, K. Jomová, I. Chodák, FTIR spectroscopy study of polyamide-6 irradiated by electron and proton beams, Polym. Degrad. Stab. 97 (2012) 523–531. doi:https://doi.org/10.1016/j.polymdegradstab.2012.01.017.

[39] H. Li, Z. Li, The effect of reactive compatibilization of carboxylated polystyrene on morphology and toughness of polyamide-1010/polystyrene blends, Polym. Int. 48 (1999) 124–128.

[40] T. Elzein, M. Brogly, J. Schultz, Crystallinity measurements of polyamides adsorbed as thin films, Polymer . 43 (2002) 4811–4822. doi:https://doi.org/10.1016/S0032-3861(02)00239-2.

[41] M. Yan, H. Yang, Improvement of polyamide 1010 with silica nanospheres via in situ melt polycondensation, Polym. Compos. 33 (2012) 1770–1776.

[42] S. Rhee, J.L. White, Investigation of structure development in polyamide 11 and polyamide 12 tubular film extrusion, Polym. Eng. Sci. 42 (2002) 134–145.

[43] R. Muthuraj, M. Misra, A.K. Mohanty, Injection Molded Sustainable Biocomposites From Poly(butylene succinate) Bioplastic and Perennial Grass, ACS Sustain. Chem. Eng. 3 (2015) 2767–2776. http://dx.doi.org/10.1021/acssuschemeng.5b00646.

[44] R. Muthuraj, M. Misra, A.K. Mohanty, Biocomposite consisting of miscanthus fiber and biodegradable binary blend matrix: compatibilization and performance evaluation, RSC Adv. 7 (2017) 27538–27548. doi:10.1039/C6RA27987B.

[45] N. Sallem-Idrissi, P. Van Velthem, M. Sclavons, Fully Bio-Sourced Nylon 11/Raw Lignin Composites: Thermal and Mechanical Performances, J. Polym. Environ. 26 (2018) 4405–4414.

[46] P.R.S. Bittencourt, D.M. Fernandes, M.F. Silva, M.K. Lima, A.A.W. Hechenleitner, E.A.G. Pineda, Lignin modified by formic acid on the PA6 films: evaluation on the morphology and degradation by UV radiation, Waste and Biomass Valorization. 1 (2010) 323–328.

[47] B.K. Kandola, S. Horrocks, A.R. Horrocks, Evidence of interaction in flame-retardant fibre-intumescent combinations by thermal analytical techniques, Thermochim. Acta. 294 (1997) 113–125.

[48] A.F. Holdsworth, A.R. Horrocks, B.K. Kandola, Synthesis and thermal analytical screening of metal complexes as potential novel fire retardants in polyamide 6.6, Polym. Degrad. Stab. 144 (2017) 420–433.

[49] X. Huang, Fabrication and Properties of Carbon Fibers, Materials . 2 (2009) 2369–2403. doi:10.3390/ma2042369.

[50] G. Szabó, D. Kun, K. Renner, B. Pukánszky, Structure, properties and interactions in ionomer/lignin blends, Mater. Des. 152 (2018) 129–139.

doi:https://doi.org/10.1016/j.matdes.2018.04.050.

[51] D. Feldman, D. Banu, Interactions in poly (vinyl chloride)–lignin blends, J. Adhes. Sci. Technol. 17 (2003) 2065–2083.

[52] K.L. Hoy, New values of solubility parameters from vapor pressure data, J. Paint Technol. 42 (1970) 76.

[53] F. Walha, K. Lamnawar, A. Maazouz, M. Jaziri, Biosourced blends based on poly (lactic acid) and polyamide 11: Structure–properties relationships and enhancement of film blowing processability, Adv Polym Tech. 37 (2018) 2061-2074.

[54] G.Wu, D.U. Shah, E-R. Janeček, H.C. Burridge,T.P. S. Reynolds, P.H. Fleming, P. F. Linden, M.H. Ramage, O.A. Scherman, Predicting the pore-filling ratio in lumen impregnated wood, 51 (2017) 1277–1290.

Captions of Tables

Table 1. Compounding temperature and compounding steps of the produced TcA blends with different bio-polyamides

Table 2. Characteristic FTIR peaks of TcA, different bio-polyamides and TcA/PA blends

Table 3. Summary of DSC analyses of TcA, different bio-polyamides and TcA/PA blends

Table 4. Summary of TGA analysis (under nitrogen) of TcA, different bio-polyamides and TcA/polyamide blends

Table 5. Group molar attraction constant, *Gm*, for TcA and bio-polyamides [52]

Table 6. Solubility parameter value of TcA and bio-polyamides as well as Gibbs free energy of the TcA/polyamide blends.

Captions of Figures

Figure 1. FTIR spectra of (a) and (b) TcA, PA11, PA1010, PA1012 and their blends; (c) and (d) TcA, PA1012 and their blends; (e) and (f); TcA, PA1010 and their blends; (g) and (h) TcA, PA11 and their blends normalised against the absorbance from 1800-1450 cm^{-1} and 1400-1150 cm^{-1}.

Figure 2. (a) DSC traces of TcA; (b) and (c) second heating scans of different bio-polyamides and TcA/PA blends; (d) and (e) first cooling scan of different bio-polyamides and TcA/PA blends and (f) crystallinity percentages in the TcA/PA blends.

Figure 3. DMA analysis (a) TcA, PA1012, and their blends; (b) TcA/PA1010 and TcA/PA11 blends

Figure 4. TGA responses of (a) TcA and blends with PA1012 and (b) TcA blends with PA11 and PA1010 under nitrogen.

Figure 5. Mass differential curves as functions of temperature for TcA/PA1012, TcA/PA1010 and TcA/PA11 blends in nitrogen.

Figure 6. Complex viscosity versus angular frequency of (a) neat TcA, bio-polyamides and (b) their blends

Figure 7. Storage modulus (G') and loss modulus (G'') versus angular frequency plots for (a) neat TcA, bio-polyamides and (b,c) TcA/PA blends (crossover points are circled)

Figure 8. SEM images of the TcA/PA blends: (a) TcA/PA1010_50/50, (b) TcA/PA1012_50/50, (c) TcA/PA11_50/50, (d) TcA/PA1010_70/30, (e) TcA/PA1012_70/30, (f) TcA/PA11_70/30 and (g) TcA domain sizes in the different blends (A: TcA/PA (50/50) and B: TcA/PA (70/30))

Figure 9. Repeating units of bio-polyamides and TcA considered for molar group attraction calculation